


## Article

# Experimental Investigation of the Effect of a Recuperative Heat Exchanger and Throttles Opening on a CO<sub>2</sub>/Isobutane Autocascade Refrigeration System

Michał Sobieraj 

Faculty of Building Services, Hydro and Environmental Engineering, Warsaw University of Technology,  
20 Nowowiejska Street, 00-653 Warsaw, Poland; [michal.sobieraj@pw.edu.pl](mailto:michal.sobieraj@pw.edu.pl); Tel.: +48-22-234-7887

Received: 7 September 2020; Accepted: 8 October 2020; Published: 12 October 2020



**Abstract:** An experimental evaluation of an autocascade refrigeration (ACR) system was carried out. A zeotropic mixture of isobutane and CO<sub>2</sub> was employed as a working fluid in an autocascade refrigeration (ACR) system. An experimental system was designed and built to study the influence of the recuperative heat exchanger (RHX) and openings of the throttle valves on the system performance. The use of RHX facilitated the condensation process and improved the cycle characteristics. The working mass concentration of CO<sub>2</sub> was higher, as it was closer to the nominal concentration and the discharge pressure was lower by 19% to even 39% when the RHX was employed in the system. An increase of up to 20% in the coefficient of performance (COP) was observed. Furthermore, the effects of the openings of the throttle valves on the system characteristics were studied. The change in the openings of the expansion valves affected the mass flows and the working mixture composition. The working CO<sub>2</sub> mass fraction increased with higher openings of the evaporator throttle. The subcooling degree of liquid CO<sub>2</sub>-rich refrigerant increased with higher openings of the expansion valve under the phase separator. The results of the present work should be helpful for design and optimization of autocascade systems working with natural and synthetic refrigerants.

**Keywords:** CO<sub>2</sub>; isobutane; R744; autocascade; natural refrigerants

## 1. Introduction

Hydrofluorocarbons (HFCs) are being phased out because of their high GWP [1]. As none of the synthetic refrigerants can be considered a long-term solution, there is an increased interest in using natural substances as refrigerants in vapor compression system [2]. Hydrocarbon (HC) refrigerants, as well as CO<sub>2</sub> (R744), possess all the properties required to make them suitable long-term replacements for fluorinated greenhouse gases [3]. However, it is the saturated vapor pressure curve that depicts the suitability of a refrigerant for given operating conditions. While the working pressure of HC-290 or HC-600a is close to that of common HFC systems, refrigerants with low critical temperature, i.e., R744 exhibit extremely high pressures and are usually employed in subcritical cascade systems allowing the condensation of the low stage refrigerant. CO<sub>2</sub> cascade systems are often used in supermarket applications in hot climates [4]. Another way to employ CO<sub>2</sub> as a refrigerant is to use a high-pressure transcritical systems. Basic flash gas bypass transcritical systems lack efficiency at high heat sink temperatures mainly because of high throttling irreversibilities [5]. Several research works have been carried out to make these systems suitable for high ambient temperature conditions, including ejectors [6] and mechanical subcooling [7].

A unique opportunity of using a high-pressure refrigerant in a subcritical operation [8] is offered by autocascade refrigeration (ACR) systems working with a zeotropic refrigerant mixture.

ACR systems were experimentally proven to be suitable for ultra-low temperature refrigeration in laboratory applications [9], including cryogenic preservation chambers [10] or in the process of natural gas liquefaction [11]. Theoretical evaluation of ACR systems operating with the binary pairs of R290/R170 and R600a/R290 for freezing application was conducted by Yan et al. [12] and Chen et al. [13]. Du et al. [14] studied an ACR system operating with a mixture of R23/R134a. The working mixture composition was reported to change in response to the opening of the throttle valves and the cooling—water temperature. Xu et al. [15] reported a change in the circulating mixture composition that resulted from changes in the openings of the throttles. An ACR system working with an additional subcooler was investigated by Chen et al. [16]. An increase in the cycle efficiency was reported. In order to boost the cycle performance, ejectors were used instead of traditional throttles [17].

Although the ACR systems have been known in the refrigeration industry for almost a century [18], very few reports can be found in the literature on the use of R744 in the ACR systems. CO<sub>2</sub> was used together with R290 and R134a to keep the discharge pressure within the limits of a subcritical operation [19]. The system was not equipped with a recuperative heat exchanger (RHX), which resulted in a low mass fraction of CO<sub>2</sub> downstream from the phase separator. Yu et al. [20] simulated the use of CO<sub>2</sub>—propane autocascade heat pump for electrical vehicles heating. The calculated COP value was higher in low-temperature ambient conditions. A modified propane/CO<sub>2</sub> ACR system with a fractionation heat exchanger (FHEX) in the form of a rectifying column in the upper section of the phase separator was investigated by Zhang et al. [21]. The FHEX improved separation efficiency, resulting in lower evaporation temperatures.

Exhaustive research work has been carried out on the characteristics of ACR systems, including: the shift of the working mixture concentration [22] and the temperature distribution in the IHXs [23]. However, there are still some gaps in the knowledge of the working principles of the ACR. Most of the abovementioned studies were carried out in the use of CFC and HFC refrigerants that are no longer available or will be banned in the nearest future. Because natural substances are to be used as refrigerants in the ACR, there is a strong need to investigate the system characteristics under different working conditions to provide a complete solution for the refrigeration industry. This work focuses on the influence of the RHX on the ACR system's characteristics, working with a novel, environmentally-friendly mixture of isobutane (R600a) and carbon dioxide (R744), providing new insight on the importance of the RHX in ACR systems. The role and the impact of the RHX on the ACR system were examined experimentally and theoretically under different condensing temperatures. The changes in the vapor quality and mass flows as well as in discharge and suction pressures were investigated. The temperature distribution (Q-T) in the internal heat exchangers (IHXs) was studied as well. Furthermore, the effect of the change in openings of the throttle valves on the system characteristics was examined. The introduction should briefly place the study in a broad context and highlight why it is important. A comprehensive study of an autocascade system was carried out, increasing the applicability range of using CO<sub>2</sub> as a refrigerant.

## 2. Experimental Setup and Procedure

The ACR's operating principle is based on the use of a zeotropic binary or a ternary mixture of refrigerants [24]. The selection of the high boiling point (HBP) and low boiling point (LBP) compounds, constituting the mixture, is based on the maximum mass fraction of the more volatile component for a given condensation pressure. The upper limit in terms of the discharge pressure for many standard HFCs compressors is 2.5 MPa.

According to Fuderer [25], the difference in the normal boiling points (NBP) of the compounds constituting the mixture should be at least 60 K. Appropriate high-boiling point (HBP) compounds can be found among HFCs (R134a, R152a, R1311), HCs (R290, R600a, R600), and hydrofluoroolefins (HFO), i.e., R1234ze.

The influence of the HBP component on the mixture's properties was studied in the author's previous work [26]. A blend consisting of isobutane (R600a) with a high mass fraction of R744 was

proposed. An HC component also serves as a solvent for dry ice, which extends the application range of CO<sub>2</sub> below the triple point temperatures [27,28]. The higher the mass fraction of CO<sub>2</sub>, the lower the temperature glide experienced during the evaporation process. Moreover, blends with higher R744 mass content can be regarded as being significantly safer in terms of flammability limits [29]. The maximum mass fraction of the high-pressure gas R744 was calculated to be 50% with a condensing temperature of 35 °C and the discharge pressure of 2.5 MPa. Based on the Le Chatelier's method [30] and the experimental data by Tian et al. [31], the proposed mixture of isobutane and carbon dioxide exhibits flammability until the concentration of the inert CO<sub>2</sub> is as high as 92%. Thus, the studied mixture of R744/R600a is classified in A3 group as per ASHRAE Standard 34.

According to Figure 1, the experimental setup consists of a 19.3 cm<sup>3</sup> compressor, an oil separator, a water-cooled coaxial condenser, coaxial heat exchangers, and electronic expansion valves (EV<sub>A</sub> and EV<sub>B</sub>) and an electrically heated evaporator. The internal heat exchangers (CHX) are made of 1/4" OD tube in an outer shell of 1/2" OD tube, with the length of the cascade heat exchanger (CHX) and RHX being 4950 mm and 4000 mm, respectively. The chilled water is supplied to the water-cooled condenser with a pump. A manual by-pass valve, V3, is installed in the water loop in the suction side of a liquid pump to control the temperature of the water at the inlet to the condenser. This feature permits to attain the desired temperature of the partially condensed zeotropic mixture, leaving the condenser (Point 3).

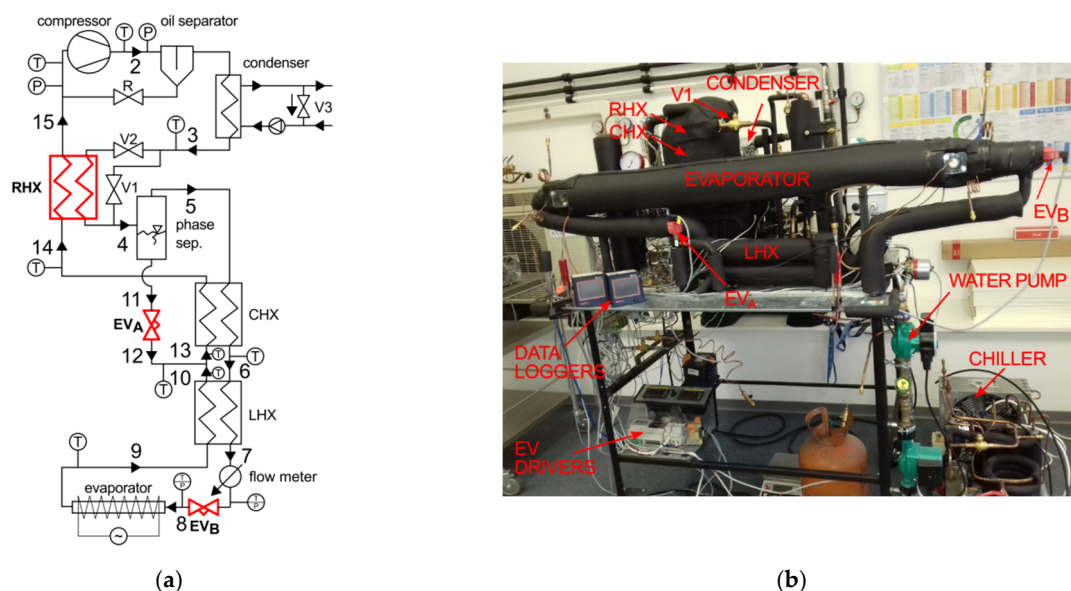


**Figure 1.** Autocascade system: (a) schematic diagram, (b) experimental stand.

The superheated vapor composed of R744/R600 (50/50 % by mass), represented by point 15 in Figure 2, is compressed to the pressure of 1.5 MPa (state 2). The refrigerant enters the water-cooled condenser, where it is partially condensed to state 3. The condensation process may be continued further in the RHX, depending on the configuration of valves V1 and V2. The mixture is separated at Point 4, at which the total wet vapor mass stream,  $\dot{m}$ , is split into the saturated liquid stream denoted as  $\dot{m}_1$  or  $\dot{m}'$ , and the saturated vapor stream that is rich in R744, denoted as  $\dot{m}_2$  or  $\dot{m}''$ . As shown in Figure 3, stream  $\dot{m}_2$  (state 5) is directed to the cascade heat exchanger (CHX), where it is condensed to a subcooled liquid (state 7). The stream  $\dot{m}_2$  is throttled in the electronic expansion valve, EV<sub>B</sub>, to state 8. The temperature conditions are below that of the R744 triple point. Isobutane (R600a) acts as a solvent for the solid R744. A strict relationship exists between the solid solubility and the solution temperature. When the process temperature is low enough, crystallisation may occur (freezing line marked blue in Figure 3). The mixture is partially sublimated and evaporated in the evaporator (state 8→9). The partially evaporated vapor is then mixed with the throttled liquid stream,  $\dot{m}_1$ , rich in R600a (state 12),

at the mixing point (state 13). The composition of the mixture at this point is equal to the charging composition. The total mass stream,  $\dot{m}$ , is evaporated in the CHX. The non-isothermal evaporation (state 13→14) is used to condense the R744-rich vapor (state 5→6). After being further evaporated in the RHX (14→15) to condense the stream leaving the water-cooled condenser, the superheated vapor (15) is aspirated by the compressor.

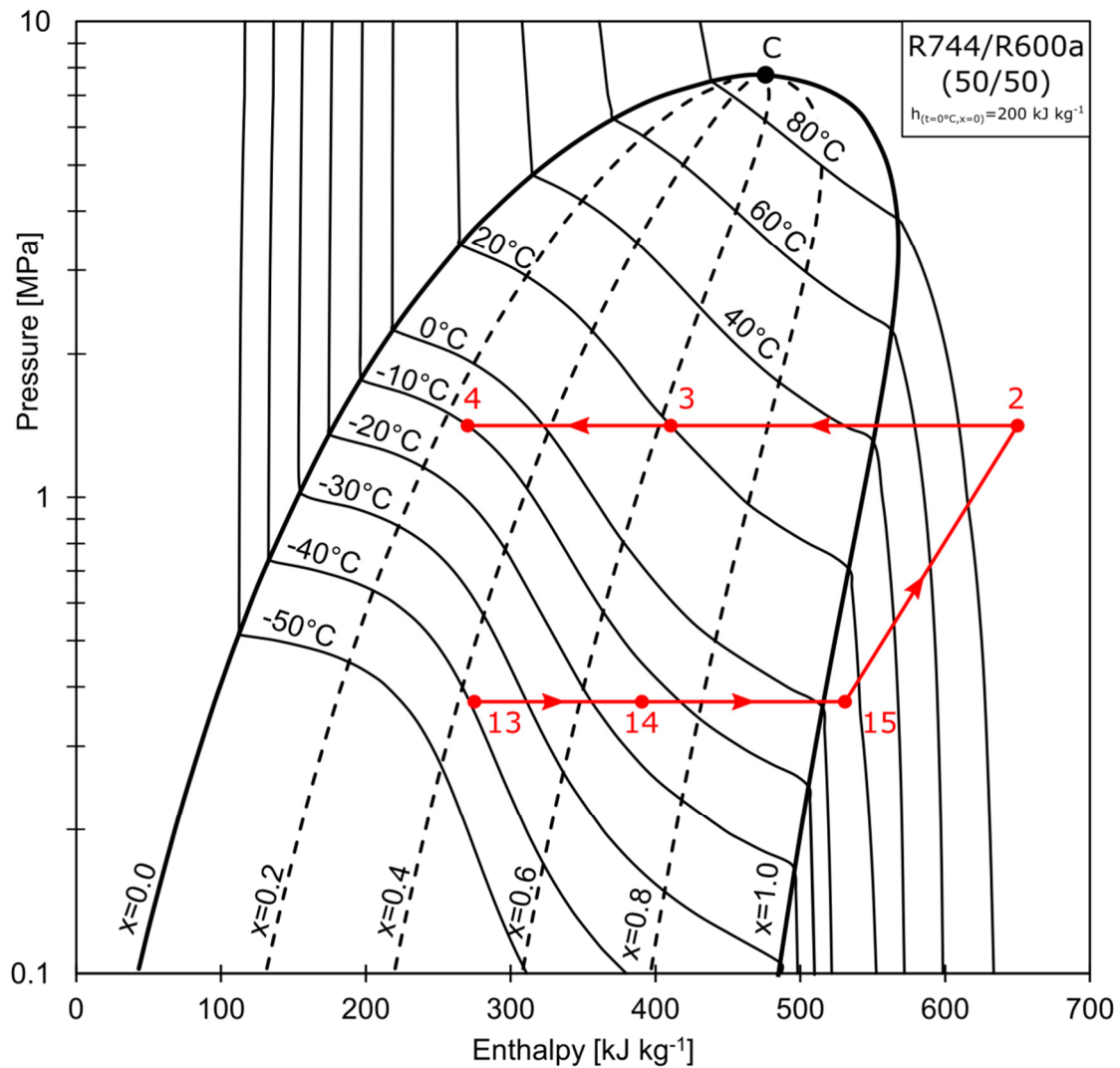


Figure 2. Pressure-enthalpy graph of ACR.

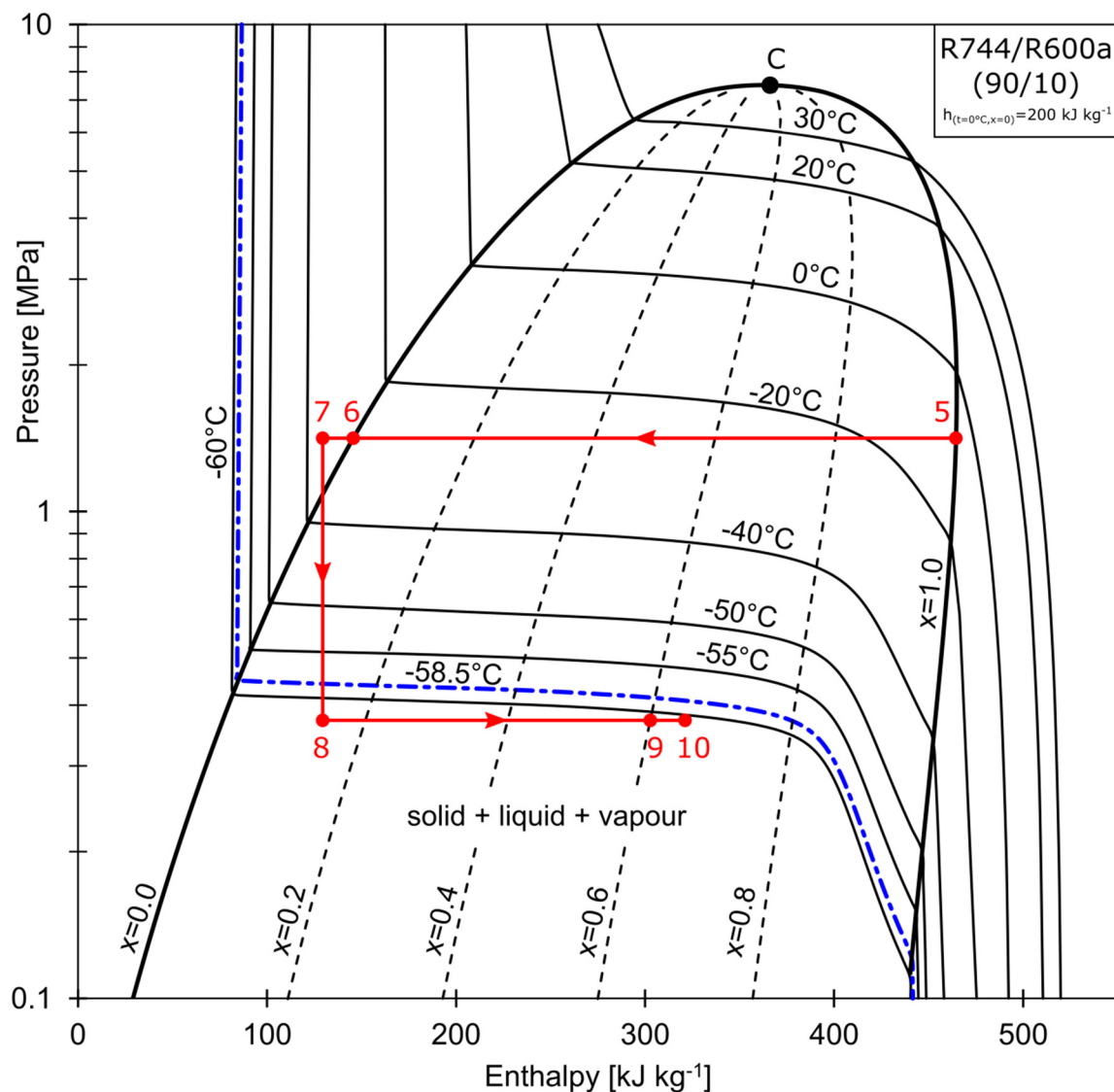


Figure 3. Phase changes of high CO<sub>2</sub> concentration mass flow.

A data acquisition system consisting of two multichannel data loggers was used to register the system parameters. Power transducers, with an uncertainty of  $\pm 2.0$  W, were used to measure the compressor power as well as the power delivered to the evaporator test section. The combined standard uncertainty in the coefficient of performance (COP) was given by the following equation:

$$u_c(COP) = \sqrt{\left(\frac{\partial COP}{\partial \dot{Q}}\right)^2 u^2(\dot{Q}) + \left(\frac{\partial COP}{\partial W}\right)^2 u^2(W)} \quad (1)$$

With the coverage factor of 2, the expanded relative uncertainty in COP was  $\pm 2.5\%$ .

The temperatures were measured with three—wire miniature PT100 resistors with an uncertainty of  $\pm 0.1$  K. The gauge pressure was measured with piezoelectric pressure transducers having an uncertainty of  $\pm 1.2\%$  of the full-scale (FS) reading, with an FS within the range of 0 barg to 34.5 barg for the high-pressure side, while for the low pressure, transducers with a FS ranging from  $-1$  barg to 9.3 barg were used. A DI3 Coriolis—effect mass flow meter with an uncertainty of  $\pm 0.1\%$  was used to measure the mass flow of the R744-rich fraction. The CO<sub>2</sub> mass fraction in the R744-rich stream was measured by introducing the liquid refrigerant into a pressure vessel, where the temperature and the



pressure were measured. For a given binary mixture, based on the Raoult's law and Dalton's partial pressures law, the composition was calculated using REFPROP from the measured temperature and pressure. The composition estimation uncertainty was calculated based on the uncertainties of the temperature measurement and the pressure measurement uncertainties and was calculated using the following equation:

$$u_c(\xi) = \sqrt{\left(\frac{\partial \xi}{\partial T}\right)^2 u^2(T) + \left(\frac{\partial \xi}{\partial p}\right)^2 u^2(p)} \quad (2)$$

The relative uncertainty in the composition calculation was  $\pm 0.2\%$ . The method is described in detail in US Patent US518601 and was verified here in this study in a series of tests regarding the R744 solubility, in which the calculated composition matched perfectly with the onset of the crystallization process. The composition in the other points of the system was calculated from the measured temperatures and pressure based on the developed autocascade mathematical model. Table 1 summarises the experimental uncertainties.

**Table 1.** Summary of experimental uncertainties.

| Parameter                  | Uncertainty    |
|----------------------------|----------------|
| Temperature                | $\pm 0.1$ K    |
| Pressure (high side)       | $\pm 0.41$ bar |
| Pressure (low side)        | $\pm 0.12$ bar |
| Power                      | $\pm 2$ W      |
| Mass flow rate             | $\pm 0.1\%$    |
| Evaporator heat load       | $\pm 1.0\%$    |
| Coefficient of performance | $\pm 2.5\%$    |
| Vapour quality             | $\pm 3\%$      |
| Composition                | $\pm 0.2\%$    |

### 3. Results and Discussion

#### 3.1. RHX and Condensing Temperature

The experimental ACR system was charged with 560.9 g of R744/R600a (51.6% of R744 by mass). The refrigerants were charged separately, with R600a as a low-pressure refrigerant is charged first. According to Bai et al. [22] and former experimental results, the working mass concentration of the more volatile component, R744, is usually lower than the charging concentration. For this reason the system was charged with the mixture containing more R744 to attain the working concentration closer to the desired one.

The heat load of the evaporator was held at a constant value of 136 W. An analysis of the impact of the condensing temperature and the use of RHX on the ACR unit was conducted. The condensing temperature was maintained at values of: 20 °C, 25 °C, 30 °C, 35 °C. A series of experiments was conducted with and without the RHX. The expansion valves (EV<sub>A</sub> and EV<sub>B</sub>) were 60% open. Each time there was a change made in the system configuration, it took some time for the unit to reach a steady-state operation. At that point, the parameters were measured every 5 s for 10 min and then the average values were calculated.

Figure 4 shows the system parameters during the start-up and the series of experiments that followed. The compressor was started at 7:31. The ACR reached the evaporation temperature,  $T_8$ , of  $-58.5$  °C after eight minutes of operation. At this point, the evaporator heater was turned on. When  $T_8$  was  $-61.0$  °C at 7:50, the temperature fluctuations, marked as (a) could be noticed. This phenomenon was caused by a crystallisation of dry ice in a supersaturated solution. A steady-state was reached at

8:05 with a corresponding condensing temperature,  $T_3$ , of 20 °C. The measurements taken from 8:15 to 8:25 were selected as the first result of the experimental series. The condensing temperature,  $T_3$ , was gradually changed until it reached the value of 35 °C. The experiments are marked with vertical lines and numbered from 1 to 8.

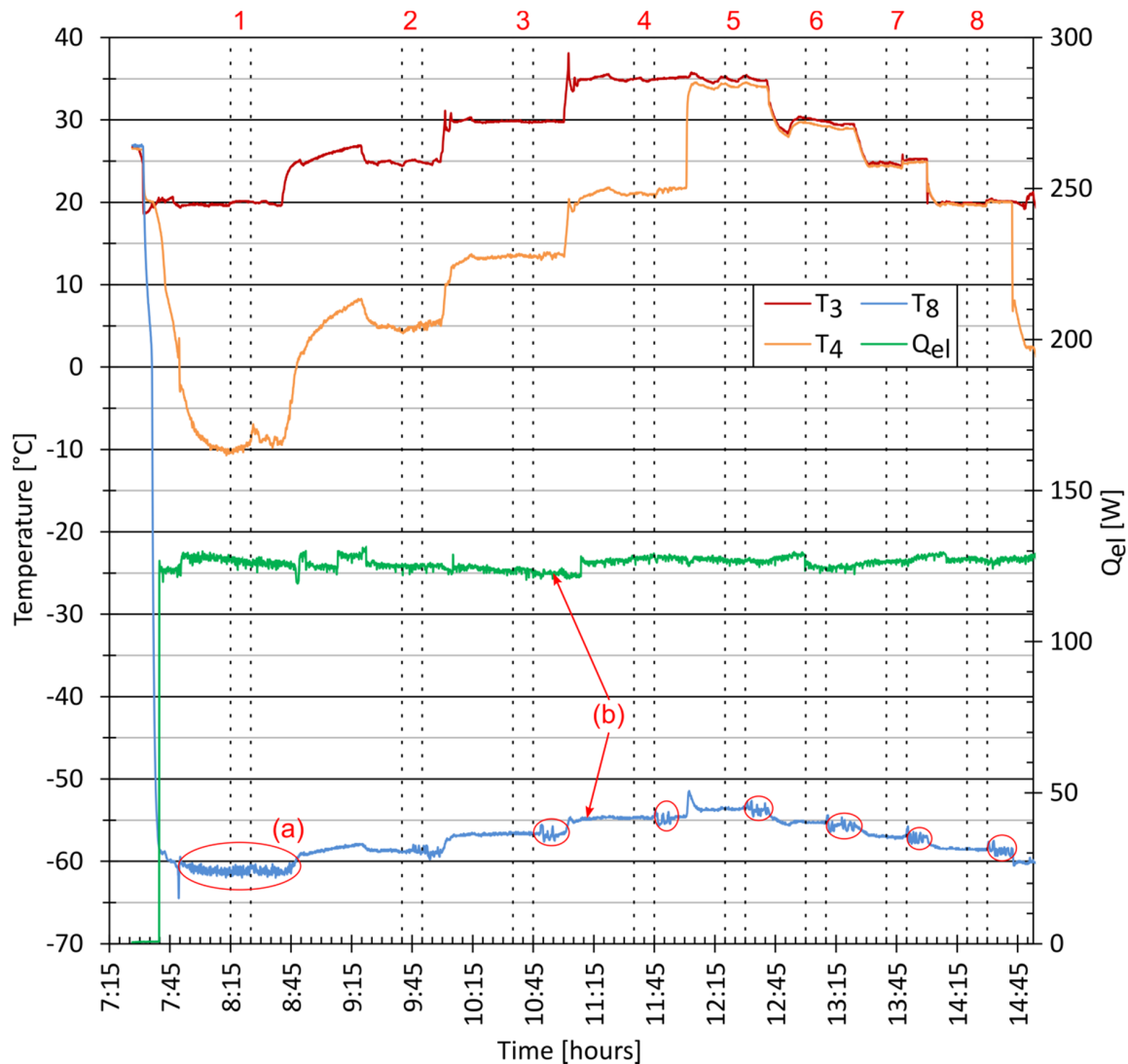


Figure 4. Experimental series—condensing temperature and RHX.

The temperature  $T_8$  gradually rose with the change in the condensing temperature. A small decrease in the heater power was observed, which was due to the increase in the heating wire resistance. In the first series  $Q_{el}$  was 127 W, but after the third series it was 122 W as marked by (b). The power of the heater was then adjusted with a TRIAC regulator to match the set value.

After experiment number 4, valves V1 and V2 were set in the correct order to deactivate the hot side of the RHX. The temperature,  $T_4$ , immediately reached the value close to  $T_3$  that was the temperature of the stream leaving the water condenser. A small difference of 0.7 K was noticed between  $T_3$  and  $T_4$  owing to the heat transfer with the surrounding air. The ambient temperature,  $T_a$ , was in the range of 23 °C to 25 °C. With lower  $T_3$  values, the difference was smaller, reaching zero at  $T_3 = 20$  °C, indicating that there was no heat exchange in this piping section.

The system parameters during the series of experiments described above are summarized in Figure 5. The discharge pressure,  $p$ , increased linearly with the condensing temperature. When the RHX was active,  $T_3$  was 20 °C, and  $p$  was 1.357 MPa; with  $T_3 = 35$  °C, the pressure  $p$  was 1.887 MPa. Turning the RHX

off, caused an increase in the discharge pressure to 1.887 MPa at  $T_3 = 20\text{ }^{\circ}\text{C}$  and to 2.248 at  $T_3 = 35\text{ }^{\circ}\text{C}$ . Former studies [19] also revealed that when there was no RHX in the ACR, the high pressure side can reach almost 3 MPa, even though the mass fraction of  $\text{CO}_2$  was significantly lower. The influence of the RHX on the suction pressure is negligible; it exhibited a 15% rise with low condensing temperatures. The changes in the discharge pressure directly influenced the power consumption of the compressor. The coefficient of performance (COP) attained its highest value of 0.182 with the RHX. When the RHX was off, the COP was 0.151. The increase in the COP was up to 20%.

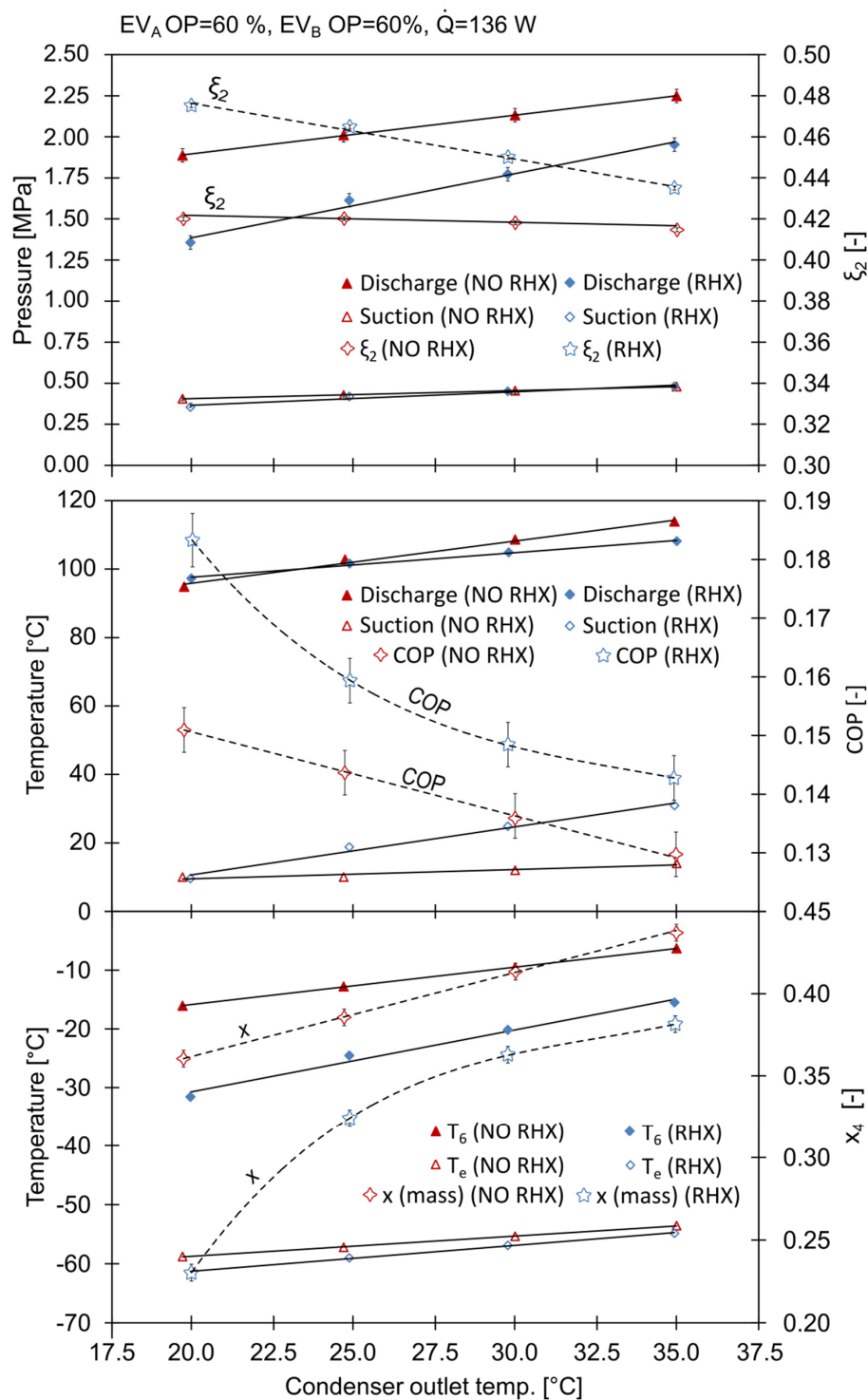


Figure 5. The influence of condensing temperature and RHX on system parameters.



The mean evaporation temperature,  $T_e$ , increased with the condensing temperature,  $T_3$ , reaching values from  $-61.4$  °C with the RHX to  $-53.6$  °C without the RHX. With low condensing temperatures, the use of the RHX reduced  $T_e$  from  $-58.8$  °C to  $-61.4$  °C.

The working mixture composition decreased with increasing condensing temperatures. The mass fraction of R744 was closest to the nominal value with the RHX active and at low  $T_3$  values, reaching a maximum of 0.455 at  $T_3 = 20$  °C. The condensing temperature had a huge impact on the mass flows in the system. As  $T_3$  increased, there was a rise in the amount of the saturated vapor leaving the phase separator.

The influence of the condensing temperature and the RHX on the vapor quality of the stream entering the phase separator is shown in Figure 6. Two different examples were illustrated. As the working composition of the mixture is usually lower than the charging composition, the mass fraction of R744 was assumed to be 0.45. In the first example denoted as (1), the condensing temperature,  $T_3$ , is 20 °C. The wet partially condensed vapor  $3_{(1)}$  is cooled in the RHX to  $T_3 = -10.3$  °C, achieving the quality  $x_{(1)} = 0.23$ . The mass fraction of R744 in the liquid phase,  $\xi'_{2(1)}$ , is 0.32, while in the vapor phase,  $\xi''_{2(1)} = 0.90$ . In the second example, when  $T_3$  is 35 °C, the wet vapor  $3_{(2)}$  flows directly into the phase separator, bypassing the RHX. As a result, less vapor is condensed, which is indicated by  $x_{(2)} > x_{(1)}$ . Both the liquid and vapor contain less R744.

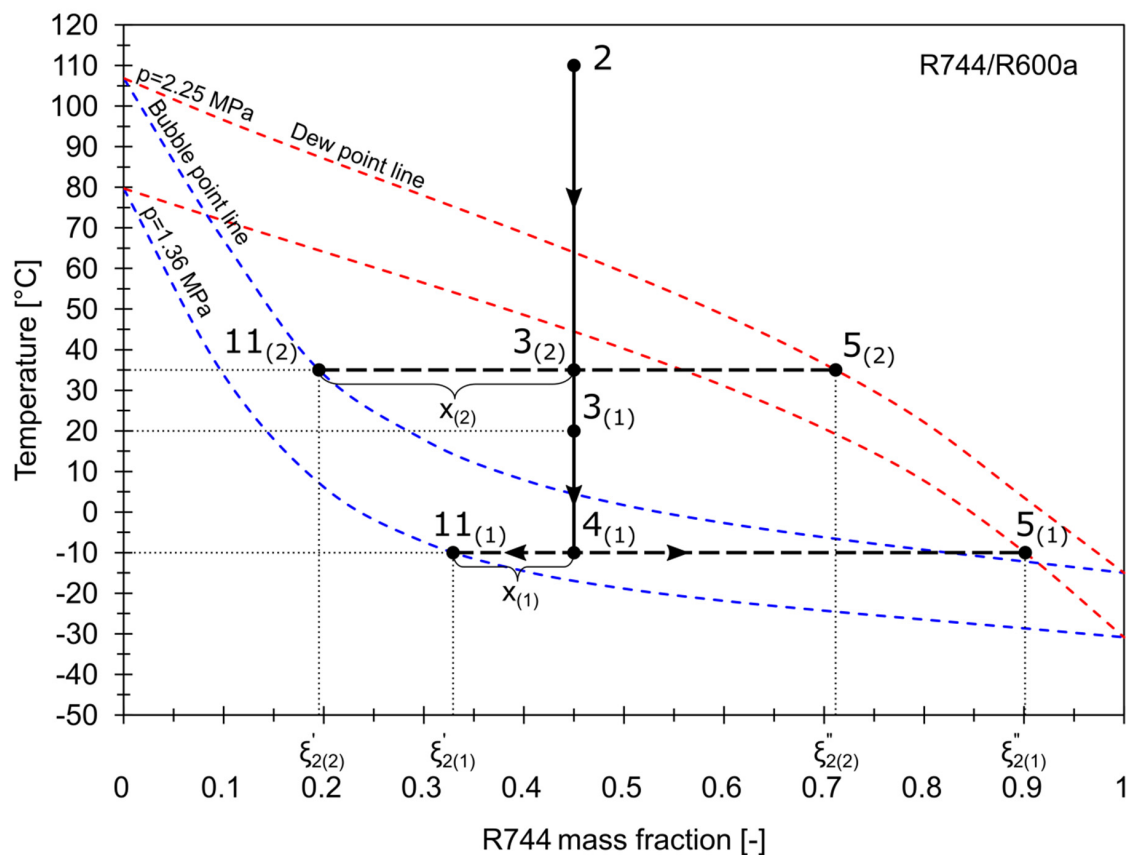


Figure 6. The influence of condensing temperature and RHX on the vapor quality.

An analysis of the temperature distribution across the IHXs was carried out. The results are presented in Table 2. The graphical interpretation in the form of Q-T diagrams is shown in Figure 7. The temperature distribution in the RHX with  $T_3 = 35$  °C is shown in Figure 7c. The vapor temperature at the inlet to the compressor  $T_1$  was 30.9 °C, which is close to  $T_3$ . The temperature difference at the RHX hot end,  $\Delta T_1^{RHX}$ , was 4.0 K, and the superheating of the refrigerant vapor leaving the RHX,  $\Delta T_{sh}^{RHX}$ , was high. The RHX was not able to transfer more heat, because of the low thermal capacity of the

stream flowing through the cold side. In this case, the temperature distribution was limited by  $\Delta T_1^{RHX}$ . As a result,  $\Delta T_2^{RHX}$  reached a high value, while the cooling capacity of the RHX was low. With lower  $T_3$  values, the temperature distribution was more favourable, as shown in Figure 7f. The thermal capacity of the cold stream was much higher, resulting in almost equal temperature differences at the ends of the IHXs.

**Table 2.** Summary of temperature differences across the IHXs.

| Series | $T_3$ | RHX          | RHX          | RHX             | CHX          | CHX          | CHX          | CHX             |
|--------|-------|--------------|--------------|-----------------|--------------|--------------|--------------|-----------------|
|        |       | $\Delta T_1$ | $\Delta T_2$ | $\Delta T_{sh}$ | $\Delta T_1$ | $\Delta T_2$ | $\Delta T_p$ | $\Delta T_{sc}$ |
|        | (°C)  | (K)          | (K)          | (K)             | (K)          | (K)          | (K)          | (K)             |
| 1      | 20.3  | 10.4         | 12.6         | 9.1             | 14.3         | 10.7         | 3.3          | 2.2             |
| 2      | 24.9  | 6.1          | 18.5         | 13.0            | 19.7         | 14.0         | 4.6          | 1.7             |
| 3      | 29.8  | 4.9          | 22.7         | 15.9            | 23.6         | 15.5         | 5.9          | 1.3             |
| 4      | 34.9  | 4.0          | 26.2         | 19.1            | 27.1         | 16.4         | 7.2          | 0.7             |
| 5      | 19.7  | 0.0          | 0.0          | 0.0             | 29.6         | 17.8         | 10.0         | 0.0             |
| 6      | 24.7  | 0.0          | 0.0          | 0.0             | 31.7         | 18.1         | 11.8         | −0.5            |
| 7      | 30.0  | 0.0          | 0.0          | 0.0             | 33.6         | 18.6         | 13.4         | −1.0            |
| 8      | 35.0  | 0.0          | 0.0          | 0.0             | 31.0         | 19.1         | 12.4         | −1.6            |

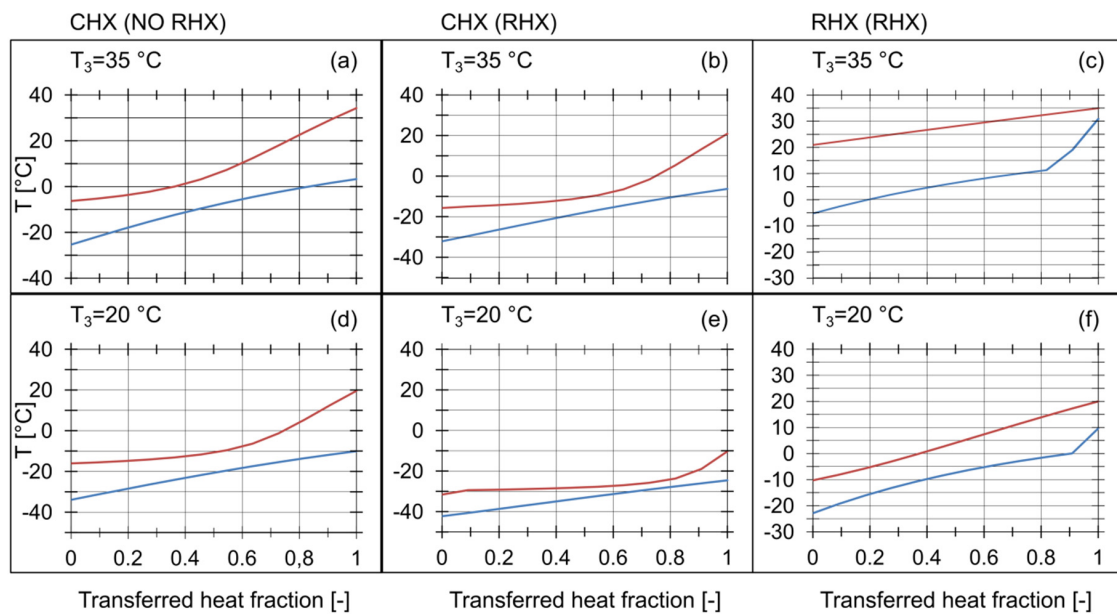


**Figure 7.** Q-T diagram for different condensing temperatures with and without the RHX across: (a) CHX without RHX at  $T_3 = 35\text{ °C}$ , (b) CHX with RHX at  $T_3 = 35\text{ °C}$ , (c) RHX with  $T_3 = 35\text{ °C}$ , (d) CHX without RHX at  $T_3 = 20\text{ °C}$ , (e) CHX with RHX at  $T_3 = 20\text{ °C}$ , (f) RHX with  $T_3 = 20\text{ °C}$ .

The use of the RHX affected the temperature distribution across the CHX. The temperature of the saturated vapor,  $T_5$ , was lower, when the RHX was active. The Q-T diagrams in Figure 7 revealed the occurrence of the pinch points between the ends of the CHX. A minimal temperature difference at the pinch point,  $\Delta T_p^{CHX}$ , was 3.3 K. There was a strict relationship between the temperature difference at the pinch point and the minimum allowable temperature approaches  $\Delta T_1^{CHX}$  and  $\Delta T_2^{CHX}$ . Thus the assumption of the temperature approaches across the IHXs should be confirmed by a detailed temperature distribution analysis as stated by Rozhenstev [23]. Otherwise very small or even negative

temperature differences at the pinch points may occur if the assumed temperature approach is relatively low in the range of 3 K to 5 K resulting in system parameters that vary from the simulated values [21].

The degree of the subcooling of the liquid refrigerant leaving the cascade condenser,  $\Delta T_{sc}^{CHX}$ , varied with the condensing temperature, and was in the range of 2.2 K to 0.7 K, with the RHX active. Turning off the RHX resulted in  $\Delta T_{sc}^{CHX}$  becoming equal to zero for  $T_3 = 20\text{ }^{\circ}\text{C}$ , and in negative values for higher condensing temperatures. It can be concluded that the condensation process was not complete without the RHX with high condensing temperatures.

### 3.2. Expansion Valves Openings

Experiments were conducted with different openings of the expansion valves  $EV_A$  and  $EV_B$ . The condensation temperature,  $T_3$ , was held at a constant value of  $20\text{ }^{\circ}\text{C}$  and the RHX was active. Preliminary tests revealed that the minimum openings were 50% for  $EV_B$  and 40% for  $EV_A$ , respectively. It was also observed that the  $EV_B$  opening should be always higher for a correct operation of the system

As shown in Table 3, the mass flow,  $\dot{m}_2$ , increased by 60% from 1.33 to 2.13 g/s with an increase in  $EV_B$  from 60% to 80%, for a constant opening of  $EV_A$  equal to 60%; while the total mass flow  $\dot{m}$  changed by 10%.

**Table 3.** Influence of expansion valves openings on mass flows.

| Mass Flow $\dot{m}_1$ (g s <sup>-1</sup> ) |    |      |      |      |
|--|----|------|------|------|
| EV   | A  |      |      |      |
|  | 40 | 50   | 60   |      |
| B  | 80 | 4.55 | 4.62 | 4.78 |
|  | 70 | 4.56 | 4.65 | 4.75 |
|  | 60 | 4.45 | 4.84 | 4.94 |
| Mass Flow $\dot{m}_2$ (g s <sup>-1</sup> ) |    |      |      |      |
| EV   | A  |      |      |      |
|  | 40 | 50   | 60   |      |
| B  | 80 | 2.42 | 2.31 | 2.13 |
|  | 70 | 2.18 | 2.07 | 1.95 |
|  | 60 | 1.83 | 1.49 | 1.33 |
| Mass Flow $\dot{m}$ (g s <sup>-1</sup> )   |    |      |      |      |
| EV   | A  |      |      |      |
|  | 40 | 50   | 60   |      |
| B  | 80 | 6.97 | 6.93 | 6.92 |
|  | 70 | 6.74 | 6.72 | 6.70 |
|  | 60 | 6.28 | 6.34 | 6.26 |

The opening of the  $EV_B$  had an effect on both the amount of the vapor leaving the separator and the total mass flow through the compressor. It should be noted that the mass content of R744 is the highest in the stream  $\dot{m}_2$ . Therefore it was the  $\dot{m}_2$  mass flow that influenced the working mixture composition mostly. While the total amount of the refrigerants charged remained unchanged, the mass percentage of  $\text{CO}_2$  in the total mass stream can be calculated with the following expression given by Du et al. [14]:

$$\xi_2 = \frac{\dot{m}_1 \xi'_2 + \dot{m}_2 \xi''_2}{\dot{m}_1 + \dot{m}_2} \quad (3)$$

The concentration of R744 in the working mixture, denoted as  $\xi_2$  in Figure 8, increased with the opening of  $EV_B$ , proving the abovementioned statements regarding the behaviour of the working concentrations. Similar results were reported by Xu et al. [15].

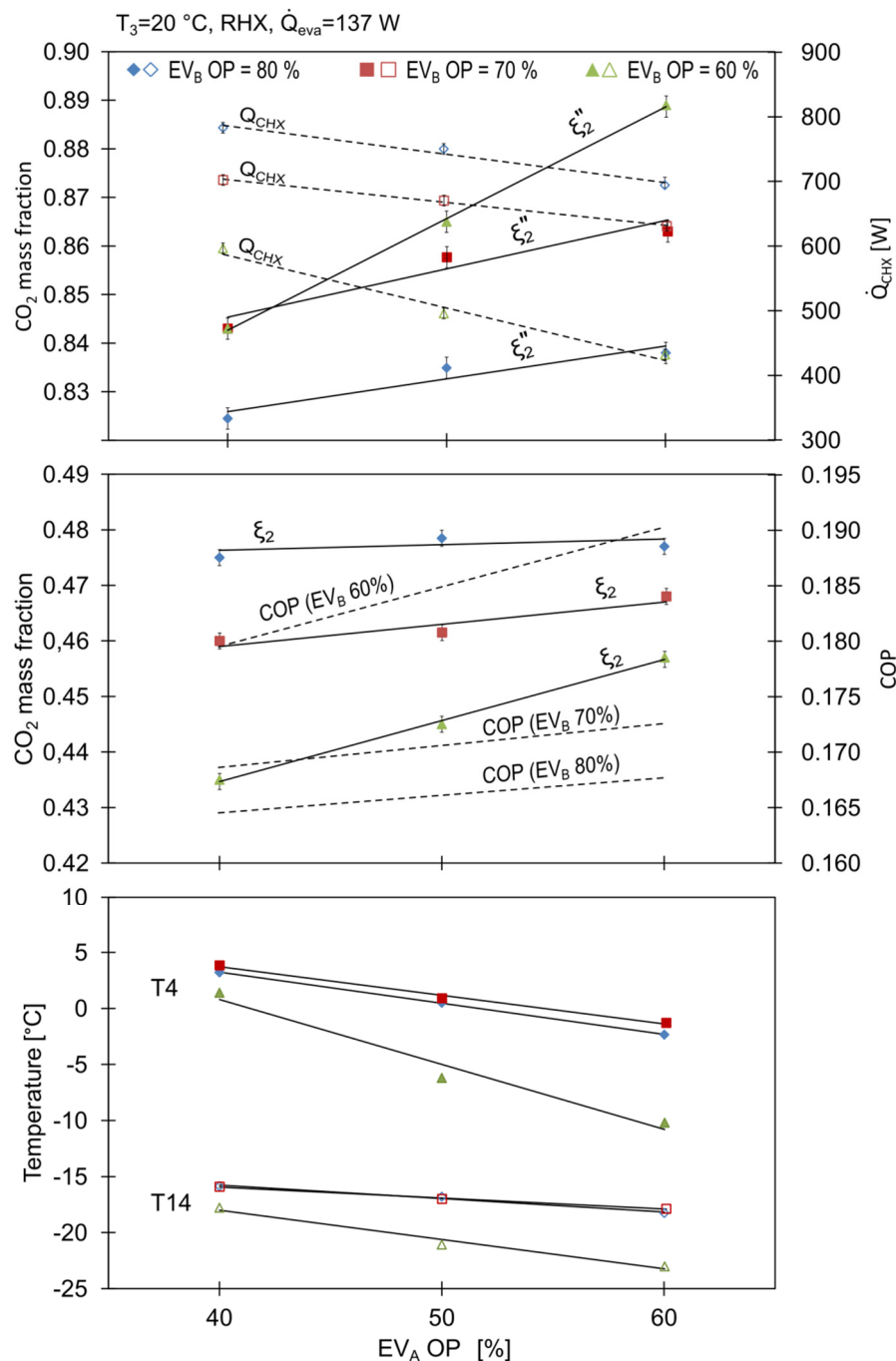


Figure 8. Influence of expansion valves openings on cycle characteristics.

It can be noticed that the temperature  $T_4$  at the separator inlet decreased with the opening of  $EV_A$ , which was a result of more liquid refrigerant stream  $\dot{m}_1$  being delivered to the mixing point 13 leading to an increase in the heat transfer rate in the CHX and RHX.

The degree of subcooling of the  $CO_2$ -rich fraction,  $\Delta T_{sc}^{CHX}$ , was altered by the openings of the expansion valves, as shown in Figure 9. Due to the changes in the mass flows  $\dot{m}_1$  and  $\dot{m}_2$ , i.e., the

increase of EVA opening with the decrease in EVB opening resulted in a lower required CHX heat transfer duty, which for a constant heat transfer area led to an increase of the subcooling degree.

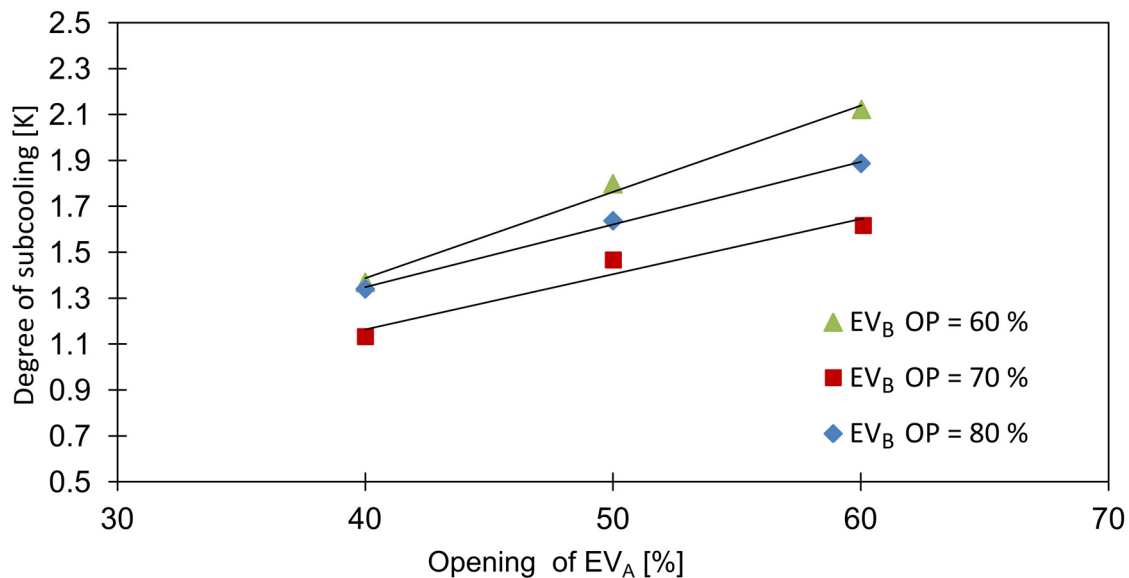


Figure 9. Influence of expansion valves openings on subcooling degree.

#### 4. Conclusions

An experimental evaluation of the ACR system was carried out. An environmental-friendly mixture of R744/R600a was employed as a working fluid. The ACR system operated at evaporation temperatures lower than the triple point of CO<sub>2</sub>. The effect of the condensing temperature and the RHX on the cycle performance was examined. The following conclusions were drawn:

The condensing temperature affected the system parameters. The discharge pressure and compressor input power increased with increasing condensing temperature. An opposite trend was observed regarding the working mass fraction of the components constituting the mixture, which became lower with higher condensing temperatures.

An analysis of the temperature distribution across the IHXs was carried out. An occurrence of the temperature pinch points was revealed. The minimal temperature difference at the pinch point,  $\Delta T_p^{CHX}$ , was 3.3 K, while much higher values were observed at the ends of the heat exchanger. The temperature approaches  $\Delta T_1^{CHX}$  and  $\Delta T_2^{CHX}$  are limited by the value of  $\Delta T_p^{CHX}$ . The use of the RHX improved the cycle performance, resulting in lower values of the discharge pressure and compressor input power. An increase in the COP of the system that reached a maximum of 20% was observed. The condensation process of the R744-rich fraction occurred properly, resulting in the subcooled liquid leaving the CHX. When the RHX was not active, the condensation process was incomplete.

When the ACR system is to run at high ambient temperatures, the use of RHX may be necessary to provide stable working conditions. Otherwise, a flash gas may be present in the liquid line, which leads to poor system performance. Moreover, the RHX helps to keep the discharge pressure within the safety limits. The opening percentage of the expansion valves has significant effect on the ACR characteristics, influencing mostly the vapor quality at the separator inlet and the working mixture composition.

It can be concluded that the overall system performance was boosted with the RHX. The results show that using the RHX in an autocascade system working under high condensing temperature may be crucial to attain the desired system parameters, including the working concentration, evaporation temperature and discharge pressure.

An autocascade system was examined, proving the possibility of utilizing a natural refrigerant CO<sub>2</sub> along with isobutane as a working binary pair for further development of environmental-friendly refrigeration systems.



While this work focused on a mixture of isobutane and carbon dioxide, further studies are needed to investigate the ACR system characteristics working with other interesting low-GWP mixtures composed of HCs, HFOs or ethers.

**Funding:** This work was supported by Faculty of Building Services, Hydro and Environmental Engineering, Warsaw University of Technology (grant numbers 504/02101/1110/42.000100 and 504/02646/1110/42.000100).

**Conflicts of Interest:** The author declares no conflict of interest.

## Nomenclature

### Symbols

|            |                                |
|------------|--------------------------------|
| $h$        | enthalpy (J kg <sup>-1</sup> ) |
| $\dot{Q}$  | heat transfer rate (W)         |
| $p$        | pressure (bar)                 |
| $W$        | compressor input power (W)     |
| $T$        | temperature (°C)               |
| $\Delta T$ | temperature difference (K)     |
| $x$        | vapor quality (mass basis) (-) |

### Greek Symbols

|       |                   |
|-------|-------------------|
| $\xi$ | mass fraction (-) |
|-------|-------------------|

### Subscripts

|      |                              |
|------|------------------------------|
| 1    | high boiling-point component |
| 2    | low boiling-point component  |
| $sc$ | subcooling                   |
| $sh$ | superheating                 |
| '    | saturated liquid             |
| ''   | saturated vapor              |

### Abbreviations

|     |                             |
|-----|-----------------------------|
| CHX | cascade heat exchanger      |
| OD  | outer diameter              |
| RHX | recuperative heat exchanger |

## References

1. European Commission. *Regulation (EU) No 517/2014 of the European Parliament and of the Council of 16 April 2014 on Fluorinated Greenhouse Gases and Repealing Regulation (EC) No 842/2006 Text with EEA Relevance*; European Commission: Brussels, Belgium, 2014.
2. Ciconkov, R. Refrigerants: There is still no vision for sustainable solutions. *Int. J. Refrig.* **2018**, *86*, 441–448. [[CrossRef](#)]
3. Lorentzen, G. The use of natural refrigerants: A complete solution to the CFC/HCFC predicament. *Int. J. Refrig.* **1995**, *18*, 190–197. [[CrossRef](#)]
4. Karampour, M.; Sawalha, S. State-of-the-art integrated CO<sub>2</sub> refrigeration system for supermarkets: A comparative analysis. *Int. J. Refrig.* **2018**, *86*, 239–257. [[CrossRef](#)]
5. Catalán-Gil, J.; Nebot-Andrés, L.; Sánchez, D.; Llopis, R.; Cabello, R.; Calleja-Anta, D. Improvements in CO<sub>2</sub> booster architectures with different economizer arrangements. *Energies* **2020**, *13*, 1271. [[CrossRef](#)]
6. Haida, M.P.; Fingas, R.; Szajnoch, W.; Smolka, J.; Palacz, M.; Bodys, J.; Nowak, A.J. An object-oriented R744 two-phase ejector reduced-order model for dynamic simulations. *Energies* **2019**, *12*, 1282. [[CrossRef](#)]
7. Nebot-Andrés, L.; Calleja-Anta, D.; Sánchez, D.; Cabello, R.; Llopis, R. Thermodynamic analysis of a CO<sub>2</sub> refrigeration cycle with integrated mechanical subcooling. *Energies* **2019**, *13*, 4. [[CrossRef](#)]
8. Stoecker, W.F. *Industrial Refrigeration Handbook*; McGraw-Hill: New York, NY, USA, 1998.
9. Aprea, C.; Maiorino, A. Autocascade refrigeration system: Experimental results in achieving ultra low temperature. *Int. J. Energy Res.* **2009**, *33*, 565–575. [[CrossRef](#)]
10. Gong, M.; Wu, J.; Cheng, Q.; Sun, Z.; Liu, J.; Hu, Q. Development of a −186 °C cryogenic preservation chamber based on a dual mixed-gases Joule–Thomson refrigeration cycle. *Appl. Therm. Eng.* **2012**, *36*, 188–192. [[CrossRef](#)]

11. Gong, M.; Wu, J.; Luo, E.; Qi, Y.; Zhou, Y. Study of the single-stage mixed-gases refrigeration cycle for cooling temperature-distributed heat loads. *Int. J. Therm. Sci.* **2004**, *43*, 31–41. [\[CrossRef\]](#)
12. Yan, G.; Hu, H.; Yu, J. Performance evaluation on an internal auto-cascade refrigeration cycle with mixture refrigerant R290/R600a. *Appl. Therm. Eng.* **2015**, *75*, 994–1000. [\[CrossRef\]](#)
13. Chen, Q.; Zhou, L.; Yan, G.; Yu, J. Theoretical investigation on the performance of a modified refrigeration cycle with R170/R290 for freezers application. *Int. J. Refrig.* **2019**, *104*, 282–290. [\[CrossRef\]](#)
14. Du, K.; Zhang, S.; Xu, W.; Niu, X. A study on the cycle characteristics of an auto-cascade refrigeration system. *Exp. Therm. Fluid Sci.* **2009**, *33*, 240–245. [\[CrossRef\]](#)
15. Xu, X.; Liu, J.; Cao, L. Mixed refrigerant composition shift due to throttle valves opening in auto cascade refrigeration system. *Chin. J. Chem. Eng.* **2015**, *23*, 199–204. [\[CrossRef\]](#)
16. Chen, Q.; Yu, J.; Yan, G. Performance analysis of a modified zeotropic mixture (R290/R600) refrigeration cycle with internal subcooler for freezer applications. *Appl. Therm. Eng.* **2016**, *108*, 172–180. [\[CrossRef\]](#)
17. Bai, T.; Yan, G.; Yu, J. Experimental investigation of an ejector-enhanced auto-cascade refrigeration system. *Appl. Therm. Eng.* **2018**, *129*, 792–801. [\[CrossRef\]](#)
18. Podbielniak, W.J. Art of Refrigeration. U.S. Patent 2041725, 26 May 1936.
19. Kim, S.; Kim, M.S. Experiment and simulation on the performance of an autocascade refrigeration system using carbon dioxide as a refrigerant. *Int. J. Refrig.* **2002**, *25*, 1093–1101. [\[CrossRef\]](#)
20. Yu, B.; Yang, J.; Wang, D.; Shi, J.; Chen, J. Modeling and theoretical analysis of a CO<sub>2</sub>-propane autocascade heat pump for electrical vehicle heating. *Int. J. Refrig.* **2018**, *95*, 146–155. [\[CrossRef\]](#)
21. Zhang, L.; Xu, S.; Du, P.; Liu, H. Experimental and theoretical investigation on the performance of CO<sub>2</sub>/propane auto-cascade refrigerator with a fractionation heat exchanger. *Appl. Therm. Eng.* **2015**, *87*, 669–677. [\[CrossRef\]](#)
22. Bai, T.; Yan, G.; Yu, J. Experimental research on the pull-down performance of an ejector enhanced auto-cascade refrigeration system for low-temperature freezer. *Energy* **2018**, *157*, 647–657. [\[CrossRef\]](#)
23. Rozhentsev, A. Refrigerating machine operating characteristics under various mixed refrigerant mass charges. *Int. J. Refrig.* **2008**, *31*, 1145–1155. [\[CrossRef\]](#)
24. Rui, S.; Zhang, H.; Zhang, B.; Wen, D. Experimental investigation of the performance of a single-stage auto-cascade refrigerator. *Heat Mass Transf.* **2015**, *52*, 11–20. [\[CrossRef\]](#)
25. Fuderer, A. Compression Process for Refrigeration. U.S. Patent 3203194, 31 August 1965.
26. Sobieraj, M.; Rosiński, M. High phase-separation efficiency auto-cascade system working with a blend of carbon dioxide for low-temperature isothermal refrigeration. *Appl. Therm. Eng.* **2019**, *161*. [\[CrossRef\]](#)
27. Di Nicola, G.; Polonara, F.; Stryjek, R.; Arteconi, A. Performance of cascade cycles working with blends of CO<sub>2</sub> + natural refrigerants. *Int. J. Refrig.* **2011**, *34*, 1436–1445. [\[CrossRef\]](#)
28. Sobieraj, M.; Rosiński, M. Experimental study of the heat transfer in R744/R600a mixtures below the R744 triple point temperature. *Int. J. Refrig.* **2019**, *103*, 243–252. [\[CrossRef\]](#)
29. Kondo, S.; Takizawa, S.; Takahashi, A.; Tokuhashi, K.; Sekiya, A. Flammability limits of isobutane and its mixtures with various gases. *J. Hazard. Mater.* **2007**, *148*, 640–647. [\[CrossRef\]](#)
30. Kondo, S.; Takizawa, K.; Takahashi, A.; Tokuhashi, K. Extended Le Chatelier's formula and nitrogen dilution effect on the flammability limits. *Fire Saf. J.* **2006**, *41*, 406–417. [\[CrossRef\]](#)
31. Tian, H.; Wu, M.; Shu, G.-Q.; Liu, Y.; Wang, X. Experimental and theoretical study of flammability limits of hydrocarbon–CO<sub>2</sub> mixture. *Int. J. Hydrogen Energy* **2017**, *42*, 29597–29605. [\[CrossRef\]](#)

